Phenomenological Analysis of the γNN^* Form Factors*

A. J. DUFNER AND Y. S. TSAI
Stanford Linear Accelerator Center, Stanford University, Stanford, California
(Received 20 November 1967)

The data on electroexcitation of N^* in the momentum-transfer range $-q^2=0.1$–2.33 GeV^2 have been analyzed phenomenologically, using an isobar model. Assuming only the $M1$ transition, we obtained a phenomenological form factor for the γNN^* vertex. This form factor is found to decrease much faster than the elastic nucleon form factors. This implies that the N^* has a larger spatial extension than the N.

1. INTRODUCTION

THE electroexcitation of the proton into $N^*(1236$ MeV) has been investigated both experimentally[1,2] and theoretically[3] by many people. The purpose of this paper is to analyze some[1,2] of these recent data phenomenologically, using a very simple isobar model. A simple parametrization of the problem as given in this paper is desirable for many applications such as (i) calculation of the radiative tail due to the 3-3 resonance in order to extract information from second (1525 MeV) and third (1688 MeV) resonances in the inelastic electron scattering; (ii) calculation of the contribution of the 3-3 resonance to various pair-production experiments; (iii) estimation of the contribution of the 3-3 resonance to various sum rules; and (iv) estimation of the effect of the 3-3 resonance on various other processes in which the N^* appears as a propagator in Feynman diagrams (e.g., Fig. 4). The usual analysis using dispersion techniques is not suited for this purpose because the result is too complicated. The situation is very similar to the analysis of elastic electron-proton scattering where phenomenological nucleon form factors are often very useful even though no one can derive them exactly from other known physical phenomena. The major difficulties in performing the phenomenological analysis are the following:

(1) It is difficult to estimate the nonresonance background in a model-independent way. From the prominence of the resonance peak in the data, one expects that the background should not exceed 10–25% of the curve at the resonance peak. At the resonance peak, the 3-3 resonance amplitude is imaginary and the background is expected to be mostly real. Hence the background simply adds to the 3-3 cross section. The background consists of (a) the tail of the second resonance, 1525 MeV; (b) the three Born diagrams shown in Fig. 1 with the $I=\frac{3}{2}$, $J=\frac{3}{2}$ amplitudes subtracted from these diagrams; and (c) the small non-3-3 amplitudes generated by the imaginary part of the 3-3 amplitude due to dispersion relations and crossing. These statements are model-dependent. The items (b) and (c) have been estimated in great detail by Zagury.[3] As can be seen from Zagury's numerical curves, the estimates of the background terms depend greatly upon some uncertain factors such as G_{En}. Hence we have chosen to estimate the background directly from the data graphs themselves. This may cause a 10–15% error in the 3-3 cross section at the peak. For most of the applications we have in mind, such errors are tolerable.

(2) Even though the $M1$ amplitude is expected to dominate[4] the transition $\gamma+N\rightarrow N^*$, one cannot tell from the data of electroproduction exactly how much the $Q2$ and $E2$ amplitudes contribute. We have written a general expression for N^* production including $Q2$ and $E2$ in addition to $M1$ [see Eq. (2.16)], but the formula contains too many parameters, and hence is impractical for use in our analysis. We have therefore assumed that only $M1$ contributes to the transition and obtained Eq. (2.18). All we can say is that the data available do not contradict the cross section expressed in this form.

Assuming that only $M1$ contributes to the transition, we have obtained a phenomenological fit to the transition form factor for $\gamma+N\rightarrow N^*$ from the most recent Stanford[1] and DESY[2] data. The result can be written as

$$[C_3(q^2)M_p]^2=(2.05\pm0.04)^2 \times\exp[-6.3(-q^2)^{1/2}][1+9.0(-q^2)^{1/2}]. \quad (1.1)$$

This form factor seems to decrease much faster than the nucleon form factors[5]

$$G_{Ep}{}^2=\left(\frac{G_{Mp}}{2.79}\right)^2=\left(\frac{G_{Mn}}{-1.91}\right)^2=\frac{1}{(1-q^2/0.71\ \text{GeV}^2)^4}. \quad (1.2)$$

The static theory of Fubini, Nambu, and Wataghin[6] predicts that the form factor associated with $\gamma+N\rightarrow N^*$ is proportional to $G_{MV}=G_{Mp}-G_{Mn}$. But this statement is very ambiguous, because in the static limit, a factor such as $E_i{}^*+M_p$ in the initial state of proton is auto-

* Supported by the U. S. Atomic Energy Commission.

[1] H. L. Lynch, J. V. Allaby, and D. M. Ritson, Phys. Rev. **164**, 1635 (1967). Earlier references on experimental papers can be traced back from this paper.

[2] F. W Brasse, J. Engler, E. Ganssauge, and M. Schweizer, DESY Report, No. 67/34, 1967 (unpublished).

[3] N. Zagury, Phys. Rev. **145**, 1112 (1966); **150**, 1406 (1966). Earlier references on theoretical papers can be traced back from this reference.

[4] R. H. Dalitz and D. G. Sutherland, Phys. Rev. **146**, 1180 (1966).

[5] See, for example, R. Taylor's report in the Proceedings of the International Symposium on Electron and Photon Interactions at High Energies at SLAC, 1967 (unpublished).

[6] S. Fubini, Y. Nambu, and V. Wataghin, Phys. Rev. **111**, 329 (1958).

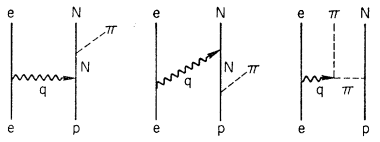

FIG. 1. The Born diagrams which contribute to the background.

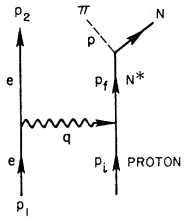

FIG. 2. Electroexcitation of the N^*.

matically replaced by $2M_p$. The result is that a kinematical factor such as

$$\frac{E_i^*+M_p}{2M_p}=\frac{(M_p+M_{33})^2}{4M_pM_{33}}\left(1+\frac{|q^2|}{(M_p+M_{33})^2}\right) \quad (1.3)$$

would be replaced by (1). (E_i^* is the energy of initial proton in the rest system of the N^*.) This factor is not small compared with unity when $|q^2|$ is 2.35 GeV^2, for example. Therefore, the static model does not predict the form factor for the γNN^* vertex at high momentum transfer. From Eqs. (1.1) and (1.2), one is tempted to conclude that the N^* has a larger radius than N, in agreement with the intuitive notion that an excited state should have a looser structure than the ground state. This observation is true even if Eq. (1.1) is multiplied by the square of the factor given by Eq. (1.3) and then the product is compared with Eq. (1.2).

In the Appendix we present in detail how the multipole analysis can be carried out, using the formalism of Durand, DeCelles, and Marr (DDM).[7] This method seems to be much more simple and straightforward than the usual way of reducing the matrix elements into a Chew-Goldberger-Low-Nambu type[3,6,8] of decomposition.

2. CALCULATIONS

In the isobar model, the relevant diagram is shown in Fig. 2, which defines our notation. P_1, P_2, P_i, and P_f are the four-momenta of the incident electron, final electron, initial proton, and N^*, respectively. q is the momentum transfer. The final pion is denoted by P. Since the initial proton has isospin $\frac{1}{2}$, spin $\frac{1}{2}$, and parity $+$, and the N^* has isospin $\frac{3}{2}$, spin $\frac{3}{2}$, and parity $+$, the transition current for $\gamma+N\rightarrow N^*$ must be isovector and has multipolarities[7] $Q2$ (scalar quadrupole), $E2$ (transverse electric quadrupole), and $M1$ (magnetic dipole). Instead of decomposing the amplitude into $M1$, $E2$, and $Q2$, one could also use the helicity amplitudes f_0, f_+ and f_- used by Bjorken and Walecka[9]; however, since in the case of $N^*(1236)$ both theoretical and experimental analyses indicate that the $M1$ amplitude dominates the cross section,[4] it is more natural to decompose the amplitude into $Q2$, $E2$, and $M1$. We shall choose the γpN^* coupling to be the sum of three gauge-invariant amplitudes[10,11]:

$$H_3=ieC_3\bar{\psi}_\nu(x)\gamma_5\gamma_\mu\varphi(x)F_{\mu\nu}+\text{H.c.}, \quad (2.1)$$

$$H_4=-eC_4\bar{\psi}_\nu(x)\gamma_5[\partial_\mu\varphi(x)]F_{\mu\nu}+\text{H.c.}, \quad (2.2)$$

$$H_5=-eC_5\bar{\psi}_\nu(x)\gamma_5\varphi(x)\partial_\mu F_{\mu\nu}+\text{H.c.}, \quad (2.3)$$

where $\varphi(x)$ is the proton field, $F_{\mu\nu}$ is the electromagnetic field tensor $F_{\mu\nu}=\partial_\mu A_\nu-\partial_\nu A_\mu$, and ψ_ν is the spin-$\frac{3}{2}$ field of Rarita and Schwinger, satisfying the subsidiary conditions[12]

$$\partial_\nu\psi_\nu=0, \quad \gamma_\nu\psi_\nu=0,$$

and

$$[i(\gamma_0\partial_0+\boldsymbol{\gamma}\cdot\boldsymbol{\nabla})-M_f]\psi_\nu(x)=0.$$

With this choice of couplings, H_5 does not contribute to the cross section when the photon is on the mass shell. C_3, C_4, and C_5 are for simplicity *assumed* to be functions of q^2 alone (but not M_f^2) in momentum space. $C_3(0)$ and $C_4(0)$ can be obtained by comparison with photoproduction experiments. The experiments of Lynch *et al.*[1] and of the DESY[2] group detect only the energy and angle of the final electrons; hence the cross section can be written in the lab system as[13]

$$\frac{d^2\sigma}{d\Omega_2 dp_2}=\frac{r_0^2m_e^2}{q^4}4E_2^2[G_2(q^2,M_f^2)\cos^2(\tfrac{1}{2}\theta)+2G_1(q^2,M_f^2)\sin^2(\tfrac{1}{2}\theta)], \quad (2.4)$$

where[14]

$$r_0=2.82\times10^{-13}\text{ cm}, \quad m_e=0.51\times10^{-3}\text{ GeV},$$

$$q^2=-4E_1E_2\sin^2(\tfrac{1}{2}\theta),$$

$$M_f^2=(q+p_i)^2=q^2+M_p^2+2q_0M_p, \quad q_0=E_1-E_2,$$

[7] L. Durand, P. DeCelles, and R. Marr, Phys. Rev. **126**, 1882 (1962). In this reference, the multipole analysis is done in the brick-wall system. Their results can easily be transformed into the rest system of the N^*.

[8] G. F. Chew, M. L. Goldberger, F. E. Low, and Y. Nambu, Phys. Rev. **106**, 1345 (1957).

[9] J. D. Bjorken and J. D. Walecka, Ann. Phys. (N. Y.) **38**, 35 (1966).

[10] M. Gourdin and Ph. Salin, Nuovo Cimento **27**, 193 (1963); **27**, 309 (1963); Ph. Salin, *ibid.* **32**, 521 (1964).

[11] J. Mathews, Phys. Rev. **137**, B444 (1965).

[12] These subsidiary conditions merely tell us that the explicit representation of ψ_ν in the rest frame of the N^* can be given in the form shown in the Appendix [see Eqs. following (A1)].

[13] We write the cross section in terms of G_1 and G_2, anticipating that our formula can be used for calculating many other things such as the radiative tail due to the 3-3 resonance [Y. S. Tsai, in *Nuclear Structure*, edited by R. Hofstadter and L. Schiff (Stanford University Press, Stanford, Calif., 1964), p. 221] or the contribution of the 3-3 resonance to pair production [S. D. Drell and J. D. Walecka, Ann. Phys. (N. Y.) **28**, 18 (1964)]. Note that the normalization used for G_1 and G_2 in this paper is slightly different from that of the above two references.

[14] The metric used in this paper is such that $P_1\cdot P_2=E_1E_2-\mathbf{P}_1\cdot\mathbf{P}_2$. The units used are $\hbar=c=1$ and $e^2/4\pi=\alpha$. Bosons are normalized such that there are $2E$ particles/cm^3 and the fermions are normalized such that there are E/M particles/cm^3, where E is the energy of the particle and M is its mass.

and the functions G_1 and G_2 are defined by

$$T_{\mu\nu}\equiv\frac{(2\pi)^3}{e^2}\sum_i\sum_f\langle f|J_\mu(0)|i\rangle^*\langle f|J_\nu(0)|i\rangle\delta^4(q+P_i-P_f)$$

$$\equiv G_1(q^2,M_f^2)(q_\mu q_\nu q^{-2}-g_{\mu\nu})+G_2(q^2,M_f^2)M_p^{-2}[P_{i\mu}-q_\mu(P_i\cdot q)q^{-2}]\times[P_{i\nu}-q_\nu(P_i\cdot q)q^{-2}], \quad (2.5)$$

where $|i\rangle$ and $|f\rangle$ represent the initial proton state and final pion nucleon system, respectively. Choosing the direction of the three-dimensional momentum transfer $\mathbf{Q}^*$ in the rest frame of N^* as the z axis, we have from Eq. (2.5)

$$G_1(q^2,M_f^2)=T_{xx}=T_{yy}=T_{++}=T_{--}\equiv T_\perp \quad (2.6)$$

and

$$G_2(q^2,M_f^2)=\frac{M_f^2}{M_f^2}\frac{q^4}{Q^{*4}}\left(T_{00}-\frac{Q^{*2}}{q^2}T_\perp\right). \quad (2.7)$$

Since G_1 is invariant, $T_\perp$ can be evaluated in any Lorentz frame.[15] T_{00} is evaluated in the rest frame of the N^*. The three-dimensional momentum transfer $\mathbf{Q}^*$ in the rest system of the N^* is related to the corresponding quantity in the lab system by

$$M_f^2Q^{*2}=M_p^2Q^2. \quad (2.8)$$

Integrating over the phase space of the N^*, and ignoring its width, we obtain from Eq. (2.5)

$$T_{00}=\frac{M_f}{e^2}\delta(M_f^2-M_{33}^2)\sum_{\lambda_f\lambda_i}|\langle\lambda_f|J_0(0)|\lambda_i\rangle|^2, \quad (2.9)$$

$$T_\perp=\frac{M_f}{e^2}\delta(M_f^2-M_{33}^2)\sum_{\lambda_f\lambda_i}|\langle\lambda_f|J_+(0)|\lambda_i\rangle|^2, \quad (2.10)$$

where λ_f and λ_i are the helicity states of the N^* and P_i, respectively. In order to take care of the finite width of the N^*, the δ function in Eqs. (2.9) and (2.10) is replaced by the absolute square of the denominator of the propagator[16] of the N^*:

$$\delta(M_f^2-M_{33}^2)\rightarrow\frac{\Gamma M_{33}\pi^{-1}}{(M_f^2-M_{33}^2)^2+\Gamma^2M_{33}^2}. \quad (2.11)$$

The width Γ is the transition probability of $N^*\rightarrow\pi+N$, and since the $\pi+N$ system is in the p state, we expect[17]

$$\Gamma\propto P^{*3},$$

where P^* is the momentum of decaying pion in the rest system of the N^*, and can be written as

$$P^{*2}=\left(\frac{M_f^2-M_p^2+\mu^2}{2M_f}\right)^2-\mu^2,$$

where $\mu=0.14$ GeV.

$\Gamma\propto P^{*3}$ if we take into account only the p-wave phase space of the decaying pions and ignore the form factor associated with the $N^*\rightarrow N+\pi$ vertex.

We have tried two expressions for $\Gamma(M_f^2)$:

$$\Gamma(M_f^2)=0.12\text{ GeV}(P^*/P_R^*)^3 \quad (2.12)$$

and[4]

$$\Gamma(M_f^2)=0.1293\text{ GeV}\frac{(0.85P^*/\mu)^3}{1+(0.85P^*/\mu)^2}, \quad (2.13)$$

where P_R^* is the value of P^* at the resonance; i.e., we let $M_f=M_{33}=1.236$ GeV.

The matrix elements in Eq. (2.9) and (2.10) can be written in terms of $Q2$, $M1$, and $E2$ as[7]

$$\sum_{\lambda_f\lambda_i}|\langle\lambda_f|J_0(0)|\lambda_i\rangle|^2=\tfrac{1}{5}(Q2)^2, \quad (2.14)$$

$$\sum_{\lambda_f\lambda_i}|\langle\lambda_f|J_+(0)|\lambda_i\rangle|^2=\tfrac{1}{3}(M1)^2+\tfrac{1}{5}(E2)^2. \quad (2.15)$$

In the Appendix we compute the $Q2$, $M1$, and $E2$ amplitudes explicitly in terms of C_3, C_4, and C_5 [see Eqs. (A5), (A6), and (A7)].

Substituting Eqs. (A5)–(A7) and (2.5)–(2.15) into Eq. (2.4), we obtain

$$\left.\frac{d^2\sigma}{d\Omega_2dp_2}\right|_{\text{lab}}=\frac{r_0^2m_e^2}{q^4}4E_2^2\frac{M_fM_{33}\Gamma\pi^{-1}}{(M_f^2-M_{33}^2)^2+\Gamma^2M_{33}^2}\frac{1}{2M_p(E_i^*+M_p)}$$
$$\times[(M_p^2/M_f^2)q^4\times\tfrac{4}{3}[-C_3+C_4M_f+C_5q_0^*]^2_{Q2}\cos^2(\tfrac{1}{2}\theta)+Q^{*2}\{\tfrac{1}{3}[(2E_i^*+2M_p+q_0^*)C_3-C_4M_fq_0^*-C_5q^2]^2_{M1}$$
$$+[q_0^*C_3-C_4M_fq_0^*-C_5q^2]^2_{E2}\}[2\sin^2(\tfrac{1}{2}\theta)-(q^2/Q^2)\cos^2(\tfrac{1}{2}\theta)]]. \quad (2.16)$$

[15] $G_1=T_\perp$ as long as P_i does not have any transverse components. This is true in the laboratory system, in the rest system of N^*, or in the brick-wall system.

[16] The numerator on the right-hand side of Eq. (2.11) is determined by requiring that the integration with respect to M_f^2 gives unity.

[17] If we assume the matrix element for $N^{++}\rightarrow p+\pi^+$ to be $gM_p^{-1}\varphi(p_f-p)p_\mu\psi_\mu(p_f)$, we obtain

$$\Gamma=\frac{1}{12\pi}\frac{E^*+M_p}{M_f}\frac{g^2}{M_p^2}P^{*3},$$

where E^* is the energy of the decayed proton. If $\Gamma=0.12$ GeV at resonance, we obtain $g^2/4\pi=16.4$, which is very close to the pion-nucleon coupling constant $g^2/4\pi=14.7$.

TABLE I. Estimates of background and errors.

$-q^2$ (GeV^2)	Background / peak	Expt error (%)	$(\Delta F^2/F^2)_{\text{expt}}$ (%)
0.1	0.15±0.05	±5	±8
0.3	0.15±0.06	±5	±9
0.5	0.15±0.06	±5	±9
0.79	0.17±0.07	±10	±13
1.57	0.18±0.07	±10	±13
2.35	0.20±0.10	±10	±15

The subscripts $Q2$, $M1$, and $E2$ at the right-hand side of each square bracket identify the contributions of each multipole to the cross section. The stars represent the quantities in the rest frame of the N^*; they can be written in terms of invariant quantities as follows:

$$E_i^* = (M_p^2 + M_f^2 - q^2)(2M_f)^{-1},$$
$$q_0^* = (M_f^2 - M_p^2 + q^2)(2M_f)^{-1},$$

and

$$Q^{*2} = q_0^{*2} - q^2.$$

If $Q2=0$ and $E2=0$, we obtain from Eq. (2.16)

$$C_5 = 0, \quad C_4 = C_3 M_f^{-1}. \tag{2.17}$$

In this case, Eq. (2.16) can be simplified into

$$\left.\frac{d^2\sigma}{d\Omega_2 dp_2}\right|_{\text{lab}} = \frac{r_0^2 m_e^2}{-q^2}\frac{E_2}{E_1}[Q^2 + (E_1+E_2)^2]\left(\frac{M_p}{M_f}\right)^2 \times \frac{q_0 + M_p + M_f}{3M_f} C_3^2(q^2) \frac{2\Gamma M_f M_{33}\pi^{-1}}{(M_f^2 - M_{33}^2)^2 + \Gamma^2 M_{33}^2}, \tag{2.18}$$

where

E_1 is the incident electron energy;
E_2 is the outgoing electron energy;

$q_0 = E_1 - E_2$; $M_{33} = 1.236$ GeV;
$q^2 = -4E_1E_2\sin^2(\frac{1}{2}\theta)$; $M_f = (q^2 + M_p^2 + 2M_p q_0)^{1/2}$;
$Q^2 = q_0^2 - q^2$; $m_e = 0.51\times10^{-3}$ GeV;
$M_p = 0.938$ GeV; $r_0 = 2.82\times10^{-13}$ cm;

and

Γ is defined in Eqs. (2.12) and (2.13).

Equation (2.16) has too many parameters, and hence it is impractical to use it for our purpose.[18] We shall assume that only $M1$ contributes to the cross section and use Eq. (2.18). Let us write the unknown function $C_3(q^2)$ as

$$C_3(q^2)M_p = AF(q^2), \tag{2.19}$$

where $F(0)=1$ and

$$A = C_3(0)M_p = 2.05\pm0.04 \tag{2.20}$$

from the Dalitz and Sutherland analysis of photoproduction experiments (see Sec. 3). We then determine $F(q^2)$ from the experimental data.[1,2] The procedure used is as follows:

(i) Let $F^2(q^2) = \exp[-a(-q^2)^{1/2}][1+b(-q^2)^{1/2}]$, and adjust a and b until Eq. (2.18) reproduces the experimental cross sections at the peak as closely as possible.

(ii) The experimental curves will, in general, be higher than the curves obtained above on both sides of the peak. We assume that the background consists of a flat part plus the tail of the second resonance. The flat part is estimated by the difference between the curve obtained in (i) and the experimental curve midway between the threshold and the peak. The tail of the second resonance at the 3-3 peak is estimated by drawing a reasonable resonance curve. The fraction of background at the peak is estimated together with rather generous error assignments, and these are given in column 2 of Table I.

(iii) The experimental form factor squared, $F^2(q^2)_{\text{expt}}$ shown in column 3 of Table II, is then obtained by subtracting the fraction of background from $F^2(q^2)$ in step (i).

(iv) The error in the experimental form factor is estimated by taking the root mean square of the errors due to estimates of background, experimental cross sections, and the coefficient A:

$$\left(\frac{\Delta F^2}{F^2}\right)_{\text{expt}} = \left[\left(\frac{\Delta(\text{background})}{\text{peak}}\right)^2 + \left(\frac{\Delta\sigma}{\sigma}\right)^2 + 4\left(\frac{\Delta A}{A}\right)^2\right]^{1/2}. \tag{2.21}$$

Δ(background)/peak is given by the ± error in column 2 of Table I; the errors in experimental cross sections, $\Delta\sigma/\sigma$, are given in column 3; and $\Delta A/A = 0.02$, as given by Eq. (2.20). Finally, $(\Delta F^2/F^2)_{\text{expt}}$ is given in column 4 of Table I.

For comparison, we give numerical values of several functions of the form $(1-q^2B^{-1})^n$ and a function $\exp[-6.3(-q^2)^{1/2}][1+9.0(-q^2)^{1/2}]$ in Table II. It is seen that $F^2(q^2)_{\text{expt}}$ goes down much faster than the elastic proton form factor which is given in column 4 ($B=0.71$ GeV^2 and $n=-4$). $F^2(q^2)_{\text{expt}}$ seems to decrease faster than the −fourth power but slower than the −fifth with increasing $|q^2|$. The exponential form seems to fit rather nicely. Figure 3 shows the comparison of the data with Eq. (2.18), using

$$C_3^2(q^2)M_p^2 = (2.05)^2 \times \exp[-6.3(-q^2)^{1/2}][1+9(-q^2)^{1/2}] \tag{2.22}$$

and Γ given by Eqs. (2.12) and (2.13). Figures 3a–3c represent the data of Lynch *et al.*, which are given in terms of

$$\frac{d^2\sigma}{d\Omega_2 dp_2}\left[\frac{\alpha}{4\pi^2}\frac{K}{|q^2|}\frac{E_2}{E_1}\left(2+\frac{\cot^2(\frac{1}{2}\theta)}{1-q_0^2/q^2}\right)\right]^{-1} \tag{2.23}$$

versus $K \equiv (M_f^2 - M_p^2)/(2M_p)$ for fixed q^2 and E_2.

[18] See (6) of the next section.

TABLE II. Experimental form factor and various fits.

$-q^2$ (GeV^2)	$\sqrt{(-q^2)}$ (GeV)	$F^2(q^2)_{\text{expt}}$	$(1-q^2/0.71)^{-4}$	$(1-q^2/0.59)^{-4}$	$(1-q^2/0.54)^{-4}$	$(1-q^2/0.77)^{-5}$	$(1-q^2/0.75)^{-5}$	$\exp[-6.3(-q^2)^{1/2}]$ $\times[1+9(-q^2)^{1/2}]$
0.1	0.316	$(5.18\pm0.42)\times10^{-1}$	0.59	0.535	0.507	0.543	0.535	0.524
0.3	0.547	$(1.78\pm0.16)\times10^{-1}$	0.244	0.193	0.171	0.193	0.186	0.188
0.5	0.706	$(7.87\pm0.71)\times10^{-2}$	0.119	0.0858	0.0727	0.0819	0.0778	0.0856
0.79	0.89	$(2.97\pm0.39)\times10^{-2}$	0.0498	0.0331	0.0269	0.029	0.0271	0.0332
1.57	1.25	$(4.50\pm0.59)\times10^{-3}$	0.00934	0.00553	0.00426	0.00383	0.00350	0.00454
2.35	1.53	$(0.96\pm0.14)\times10^{-3}$	0.00292	0.00164	0.00123	0.000924	0.000837	0.00095

Figures 3(d)–3(f) represent DESY data which are given in terms of $d^2\sigma/d\Omega_2 dp_2$ versus P_2 for fixed θ and E_1. These curves are not only the over-all fit of our formulas and parameters but also give some idea about the shape of the background.

3. DISCUSSIONS

(1) The position of a resonance peak and the shape of the resonance curve are somewhat sensitive to the form of the width function $\Gamma(M_f^2)$ chosen. If a constant $\Gamma=0.12$ GeV were used, the resonance peak would occur at $M_f=1.236$ GeV which contradicts the data; the experimental peaks occur at $M_f\approx1.220$ GeV. Of course, a constant Γ gives a completely wrong behavior near the πN threshold. The forms of $\Gamma(M_f^2)$ given by Eqs. (2.12) and (2.13) give a theoretically correct P-wave threshold behavior but give somewhat lower values than the experimental curves near threshold. This simply means that near threshold other mechanisms such as S-wave pion electroproduction are significant. Because of large uncertainty in the background, and because of experimental uncertainties, it is impossible to judge whether Eq. (2.12) or Eq. (2.13) is better from our curves.

(2) Comparisons of fits to the data of Lynch *et al.* ($-q^2=0.1$ to 0.5 GeV^2) and DESY[2] data ($-q_{1.236}{}^2\approx0.79$ to 2.35 GeV^2) show that the experimental peaks of the data of Lynch *et al.* occur at slightly lower M_f^2 than our peaks, whereas the DESY data occur at slightly higher M_f^2 than our peaks. The experimental peak positions are affected by the background. In particular, the tail of the second resonance tends to shift the peak to the high M_f^2 side and a large S-wave contribution near threshold tends to shift the peak to the low M_f^2 side. The observed difference in the positions of the peaks between the two experimental groups may be due to the difference in the importance of the background at different q^2.

(3) The static theory of Fubini, Nambu, and Wataghin (FNW)[6] and the quark model[4] predict the form factor for the vertex γNN^* to be proportional to the isovector part of the nucleon form factor. As mentioned in the Introduction, this is a very ambiguous statement because the q^2 dependence of the proportionality constant is not specified in these theories. This seems to have caused some confusion in the literature. For example, Ash *et al.*[19] and Geshkenbein[20] made their comparisons with experiment using the relation

$$\left(1+\frac{|q^2|}{(M_f+M_p)^2}\right)^{1/2}C_3(q^2)\propto G_{MV}(q^2). \tag{3.1}$$

Bjorken and Walecka[9] inferred from the FNW[6] result

$$\left(1+\frac{|q^2|}{(M_f+M_p)^2}\right)C_3(q^2)\propto G_{MV}(q^2). \tag{3.2}$$

and Salam, Delbourgo, and Strathdee predicted on the basis of $U(6,6)$ that

$$C_3(q^2)\propto G_{MV}(q^2). \tag{3.3}$$

Our analysis of the data shows that Eq. (3.2) is closer to the truth, but $C_3(q^2)$ still goes down faster with increasing $|q^2|$ than Eq. (3.2). Intuitively, this may be just a manifestation of the fact that an excited state such as N^* has a looser structure than the ground state such as p. In quark language, this implies that there is a spin-spin coupling between two quarks $c\boldsymbol{\sigma}_1\cdot\boldsymbol{\sigma}_2$ with a positive c, so that when two quark spins are parallel they repel each other and when they are antiparallel they attract.

(4) Various estimates have been made for the constant $A=C_3(0)M_p$ from photoproduction experiments.

(a) Gourdin and Salin[10] and later Mathews[11] obtained, respectively,

$$C_3(0)M_p=2.49,$$
$$C_3(0)M_p=2.0.$$

(b) Dalitz and Sutherland[4] made a detailed analysis of the $M1$ excitation of the N^* from photoproduction, and they obtained for the radiative decay width $N_+{}^*\to p+\gamma$

$$\Gamma_\gamma=\alpha Q^{*3}(2M_pM_{33})^{-1}[(1.28\pm0.02)\tfrac{2}{3}\sqrt{2}\mu_p], \tag{3.4}$$

where $\mu_p=2.79$. For comparison, we can use our matrix element to calculate this same width as

$$\Gamma_\gamma=(Q^*/4\pi)[\tfrac{1}{3}(M1)^2+\tfrac{1}{5}(E2)^2]. \tag{3.5}$$

Setting $E2=0$, we have from Eqs. (A6) and (A7)

$$\Gamma_\gamma=\alpha C_3{}^2(0)\tfrac{2}{3}Q^{*3}(E_i{}^*+M_p)/M_{33}. \tag{3.6}$$

Equating Eq. (3.6) to Eq. (3.4), we obtain[4]

$$C_3(0)M_p=2.05\pm0.04. \tag{3.7}$$

(c) $SU(6)$ predicts[4] that the number 1.28 in Eq. (3.4)

[19] W. W. Ash, K. Berkelman, C. A. Lichtenstein, A. Ramanauskas, and R. H. Siemann, Phys. Letters **24B**, 165 (1967).
[20] B. V. Geshkenbein, Phys. Letters **11**, 323 (1965).

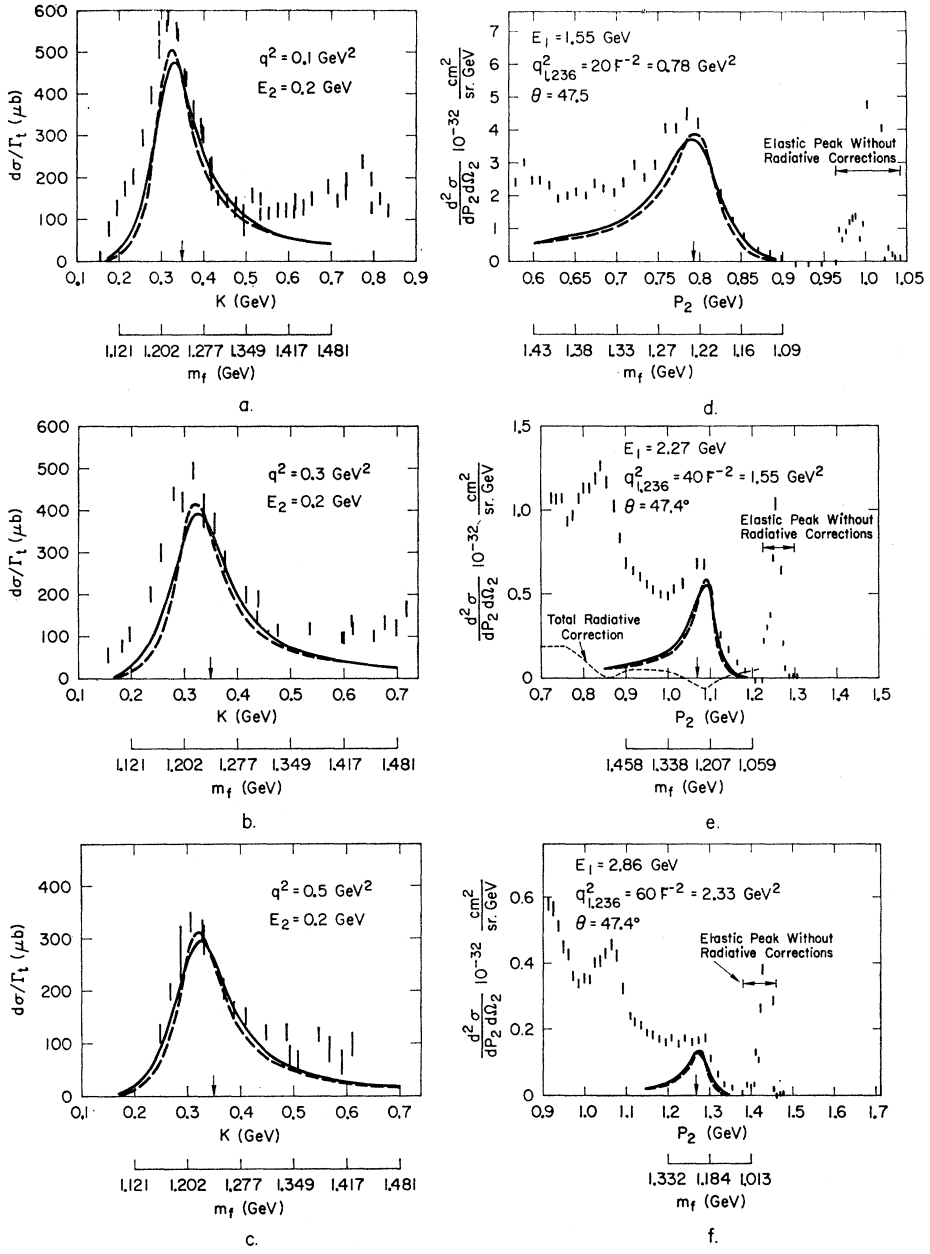

FIG. 3. Comparison of the fits using Eqs. (2.18), (2.22), and the experimental data: (a), (b), and (c) are the data of Lynch *et al.* which are given in terms of Eq. (2.26) versus $K\equiv(M_f{}^2-M_p{}^2)/(2M_p)$ for fixed q^2 and E_2; (d), (e), and (f) represent the data of Brasse *et al.* which are given in terms of $d^2\sigma/d\Omega_2 dp_2$ versus p_2 for fixed θ and E_1. Two forms of the width function Γ are illustrated. The dashed lines are obtained by using Eq. (2.12) in the cross section (2.18), and the solid lines are from Eq. (2.13). The arrow on each abscissa indicates the position of the $N^*(1.236)$ resonance. In (e), an example is given of the radiative corrections which have been applied by Brasse *et al.* to the data of (e), (f), and (g).

should be replaced by 1, hence [$SU(6)$ prediction]

$$C_3(0)M_p=1.61.$$

(d) It is also interesting to point out that we can obtain $C_3(0)M_p$ from Chew-Low static theory.[21] The relevant formula from static theory is

$$\sigma(\gamma+p\to\pi^0+p)=\left(\frac{Q^*}{P^*}\right)\left(\frac{\mu^2\alpha}{f^2}\right)\left(\frac{\mu_p-\mu_n}{4M_p}\right)^2\times\sigma(\pi^0+p\to\pi^0+p), \quad (3.8)$$

where $f^2\approx0.08$ and $\alpha=1/137$. This formula is supposed to be correct near the π^0+p threshold. In order to obtain C_3 from this relation, we compute the cross sections of both sides, using the isobar model

$$\sigma(\gamma+p\to\pi^0+p)=(M_f/M_p)16\pi^2\tfrac{1}{9}Q^*\alpha(E_i{}^*+M_p)\times C_3{}^2(0)\delta(M_f{}^2-M_{33}{}^2), \quad (3.9)$$

$$\sigma(\pi^0+p\to\pi^0+p)=(M_f{}^2/M_p)32\pi^2\tfrac{1}{9}P^{*-2}\Gamma\times\delta(M_f{}^2-M_{33}{}^2), \quad (3.10)$$

where $\Gamma=(8/3)(f^2/\mu^2)P^{*3}$ near threshold, according to static theory. Hence

$$C_3{}^2(0)=\frac{2M_f}{E_i{}^*+M_p}\frac{8}{3}\left(\frac{\mu_p-\mu_n}{4M_p}\right)^2. \quad (3.11)$$

[21] G. F. Chew and F. E. Low, Phys. Rev. **101**, 1579 (1956), Eq. (51). The units used for e^2 and f^2 are extremely confusing in this paper. One is never sure whether $e^2=\alpha$ or $e^2/4\pi=\alpha$ and whether $f^2=0.08$ or $f^2/4\pi=0.08$ or $f^2/\mu^2=0.08$. The same criticism can be applied to Ref. 6.

Now if the δ functions in Eqs. (3.9) and (3.10) are replaced by a Breit-Wigner formula, then they are also usable near threshold. Since Eq. (3.8) is more correct near threshold, we let $M_f-\mu=E_i^*=M_p$ in Eq. (3.11) and finally obtain (Chew-Low static theory)

$$C_3(0)M_p=2.2. \tag{3.12}$$

(5) Dalitz and Sutherland[4] obtained a formula for $d^2\sigma/d\Omega_2 dP_2$ from the result of Dalitz and Yennie.[22] Our Eq. (2.18) differs somewhat from their Eqs. (2.16) and (2.16′). There is an error of a factor 4π in their Eqs. (2.16) and (2.16′).[23] The forms of the Breit-Wigner formula used are different, but this is just a matter of taste.

From their Eq. (2.14) and our Eq. (3.5), the expression $\mathfrak{M}$ in Dalitz and Sutherland is related to our $C_3(q^2)$ by

$$|\mathfrak{M}|^2=\tfrac{4}{3}\pi\alpha[(E_i^*+M_p)/M_p]C_3^2(q^2). \tag{3.13}$$

Substituting Eq. (3.13) into their Eq. (2.16), we see that our Eq. (2.18) is equal to their Eq. (2.16) at $M_f=M_{33}$ except for a factor of 4π. According to Dalitz and Sutherland, their Eq. (2.16′) is better than their Eq. (2.16) because the former has an extra factor E_i^*/M_p which comes from the transformation from the rest system of the N^* to the lab system. This factor is a mystery to us because according to the way we computed the cross section, $G_1=T_1$ is invariant and hence no extra factor needs to be multiplied when we go from the N^* rest system to the lab system. However, this factor has a numerical value of 0.972/0.938 at the resonance, and hence is insignificant numerically.

(6) We have completely ignored the possible contributions from $Q2$ and $E2$ in our analysis. Inspection of Eq. (2.16) shows that this is an experimentally impossible task unless one has some model to tell him the q^2 dependence of $C_3(q^2)$, $C_4(q^2)$, and $C_5(q^2)$. If the decayed pion is detected in coincidence with the electron, one may be able to untangle this, but the theoretical details have to be worked out before one can say whether this is feasible or not. If C_3, C_4, and C_5 have roughly the same q^2 dependence, then we can conclude from our analysis and our Eq. (2.16) the following:

(A) The $Q2$ amplitude cannot be large because it has an extra factor of q^4 in its expression. If the $Q2$ amplitude were significant, the form factors for the C's must decrease much faster than the one discussed in this paper and this seems unlikely.

(B) The value of $C_5(q^2)$ must be small because it is multiplied by q^2 in $M1$ and $E2$, and our analysis shows that the cross section goes down rather rapidly with increasing $|q^2|$.

(7) In conclusion, if $E2=0$ and $Q2=0$, then G_1 and G_2 of Eq. (2.4) can be written as

$$G_1(q^2,M_f^2)=\frac{Q^2}{-q^2}G_2(q^2,M_f^2)$$
$$=\frac{\Gamma M_{33}M_f\pi^{-1}}{(M_f^2-M_{33}^2)^2+\Gamma^2M_{33}^2}Q^{*2}2C_3^2(q^2)\frac{(E_i^*+M_p)}{3M_p}. \tag{3.14}$$

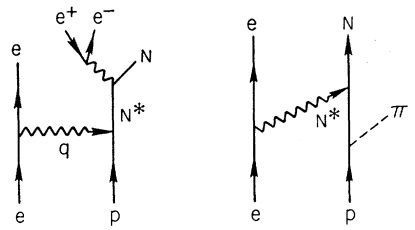

FIG. 4. Examples of Feynman diagrams which can be calculated more easily in terms of C_3, C_4, and C_5 than in terms of G_1 and G_2.

Our best fit for $C_3(q^2)$ is given by Eq. (1.1). This formula is sufficient for calculating most of the applications we have in mind, as mentioned in the Introduction. At this stage it is natural for the reader to ask why we went through all the trouble of decomposing H_3, H_4, and H_5 into multipoles instead of directly obtaining some analytical expression for G_1 by fitting the data. The reason is that there are many kinds of application of the isobar model in which it is more convenient to write expressions in terms of C_3, C_4, and C_5 than G_1 and G_2. For example, one may wish to evaluate diagrams such as are given in Fig. 4.

(8) Finally, one is tempted to ask whether form factors associated with the second resonance (1525 MeV; I, $J^\pi=\frac{1}{2},\frac{3}{2}^-$) and the third resonance (1688 MeV; I, $J^\pi=\frac{1}{2},\frac{5}{2}^+$) can be analyzed in the same fashion. Inspection of the DESY[2] data shows that it is hopeless to isolate the higher resonance contributions from the background and estimate their cross sections to within 20% accuracy. However, for many purposes a cross section known to within 20% or even 30% can be very valuable. If one wishes to do better than this, the final states of the target system must be detected in addition to the scattered electrons.

APPENDIX: MULTIPOLE ANALYSIS OF FEYNMAN DIAGRAMS

In this Appendix we illustrate how to extract multipole moments, as defined covariantly by Durand *et al.*,[7] when a relativistic vertex function is given. If the target particle has spin $\frac{1}{2}$ and the final particle has spin S, then angular momentum conservation tells us that there are at most six multipole moments $Q(S\pm\frac{1}{2})$, $M(S\pm\frac{1}{2})$, and $E(S\pm\frac{1}{2})$. Parity conservation eliminates three of the six amplitudes. For $N^*(1236)$, the relative parity between the nucleon and N^* is $+$; hence we have $Q2$, $M1$, and $E2$. Let us consider helicity amplitudes given by

[22] R. H. Dalitz and D. R. Yennie, Phys. Rev. **105**, 1598 (1957).
[23] From their Eqs. (2.13) and (2.14) their unit of e^2 must be $e^2/4\pi=\alpha$. If this is so, their Eqs. (2.16) and (2.16′) are both wrong by a factor of 4π.

the Hamiltonian of Eqs. (2.1)–(2.3):

$$\Gamma_{\lambda_f,\lambda_i}{}^{(\mu)}=\langle p_f\lambda_f|\,j_\mu|\,p_i\lambda_i\rangle$$
$$=e\bar{\psi}_\nu(p_f\lambda_f)\gamma_5[C_3(qg_{\nu\mu}-q_\nu\gamma_\mu)$$
$$+C_4(q\cdot p_f g_{\nu\mu}-q_\nu p_{f\mu})$$
$$+C_5(q\cdot p_i g_{\nu\mu}-q_\nu p_{i\mu})]\varphi(p_i\lambda_i). \quad \text{(A1)}$$

Since the spin-$\frac{3}{2}$ particle is more complicated than the spin-$\frac{1}{2}$ particle, we shall evaluate everything in the rest frame of the N^*. Let us use the explicit representation

$$\gamma_5=\begin{bmatrix}0 & 1\\ 1 & 0\end{bmatrix},\quad \gamma_0=\begin{bmatrix}1 & 0\\ 0 & -1\end{bmatrix},\quad \boldsymbol{\gamma}=\begin{bmatrix}0 & \boldsymbol{\sigma}\\ -\boldsymbol{\sigma} & 0\end{bmatrix}.$$

Then

$$\varphi(p_i\lambda_i)=\frac{1}{\sqrt{N}}\begin{bmatrix}1\\ \dfrac{\boldsymbol{\sigma}\cdot\mathbf{p}_i}{E_i+M_p}\end{bmatrix}\chi_{\lambda_i},$$

where

$$\chi_{1/2}=\alpha\equiv\begin{bmatrix}1\\ 0\end{bmatrix},$$

$$\chi_{-1/2}=\beta\equiv\begin{bmatrix}0\\ 1\end{bmatrix},$$

and

$$N=\frac{2M_p}{E_i^*+M_p}.$$

In the rest frame of the N^*, $\psi_\nu(p_f\lambda_f)$ can be written (because of the subsidiary conditions) as

$$\psi_\nu(0,\lambda_f)=|\,s,-s_z\rangle.$$

Hence

$$\psi_\nu(0,\tfrac{3}{2})=\begin{bmatrix}1\\ 0\end{bmatrix}\hat{e}_-\beta,$$

$$\psi_\nu(0,\tfrac{1}{2})=\begin{bmatrix}1\\ 0\end{bmatrix}[(\sqrt{\tfrac{2}{3}})\hat{e}_z\beta+(\sqrt{\tfrac{1}{3}})\hat{e}_-\alpha],$$

$$\psi_\nu(0,-\tfrac{1}{2})=\begin{bmatrix}1\\ 0\end{bmatrix}[(\sqrt{\tfrac{1}{3}})\hat{e}_+\beta+(\sqrt{\tfrac{2}{3}})\hat{e}_z\alpha],$$

$$\psi_\nu(0,-\tfrac{3}{2})=\begin{bmatrix}1\\ 0\end{bmatrix}\hat{e}_+\alpha.$$

In the rest frame of the N^*, we have $\mathbf{Q}^*=-\mathbf{P}_i{}^*=\hat{e}_zQ^*$ and we may evaluate the helicity amplitudes $\Gamma_{\lambda_f\lambda_i}{}^{(\mu)}$ for any combination of μ, λ_f, and λ_i immediately from these formulas. Now, using Eqs. (109), (119), and (120) of (DDM),[7] we have

$$\Gamma_{\lambda_f\lambda_i}{}^{(0)}=\begin{pmatrix}\frac{3}{2} & 2 & \frac{1}{2}\\ \lambda_f & 0 & \lambda_i\end{pmatrix}(Q2), \quad \text{(A2)}$$

$$\Gamma_{\lambda_f\lambda_i}{}^{(+1)}\quad\begin{pmatrix}\frac{3}{2} & 1 & \frac{1}{2}\\ \lambda_f & 1 & \lambda_i\end{pmatrix}(M1)-\begin{pmatrix}\frac{3}{2} & 2 & \frac{1}{2}\\ \lambda_f & 1 & \lambda_i\end{pmatrix}(E2), \quad \text{(A3)}$$

$$\Gamma_{\lambda_f\lambda_i}{}^{(-1)}=\begin{pmatrix}\frac{3}{2} & 1 & \frac{1}{2}\\ \lambda_f & -1 & \lambda_i\end{pmatrix}(M1)$$
$$-\begin{pmatrix}\frac{3}{2} & 2 & \frac{1}{2}\\ \lambda_f & -1 & \lambda_i\end{pmatrix}(E2), \quad \text{(A4)}$$

where

$$\begin{pmatrix}S_f & J & S_i\\ \lambda_f & \mu & \lambda_i\end{pmatrix}$$

is Wigner's $3J$ symbol. We may arbitrarily let $\lambda_i=\frac{1}{2}$, remembering $\lambda_f=-(\mu+\lambda_i)$, and solve for $Q2$, $M1$, and $E2$. The results are

$$Q2=-(\sqrt{10})\Gamma_{-\frac{1}{2},\frac{1}{2}}{}^{(0)}=\left(\sqrt{\frac{20}{3}}\right)\frac{eQ^{*2}}{N^{1/2}(E_i^*+M_p)}$$
$$\times(-C_3+C_4M_f+C_5q_0^*), \quad \text{(A5)}$$

$$M1=\tfrac{1}{2}(\sqrt{3}\Gamma_{\frac{1}{2},\frac{1}{2}}{}^{(-)}-3\Gamma_{-\frac{3}{2},\frac{1}{2}}{}^{(+)})=\frac{eQ^*}{N^{1/2}(E_i^*+M_p)}$$
$$\times\{[2(E_i^*+M_p)+q_0^*]C_3-C_4M_fq_0^*-C_5q^2\}, \quad \text{(A6)}$$

$$E2=-\tfrac{5}{2}(\sqrt{3}\Gamma_{\frac{1}{2},\frac{1}{2}}{}^{(-)}+\Gamma_{-\frac{3}{2},\frac{1}{2}}{}^{(+)})=\frac{e(\sqrt{5})Q^*}{N^{1/2}(E_i^*+M_p)}$$
$$\times(q_0^*C_3-C_4M_fq_0^*-C_5q^2). \quad \text{(A7)}$$

From these expressions we observe the following:

(1) Our expressions for the multipoles have the correct threshold behavior, namely, $Q2\propto Q^{*2}$, $M1\propto Q^*$, and $E2\propto Q^*$.

(2) When the photon is real, C_5 does not contribute to the cross section.

(3) Since for real photons ($q_0^{*2}-Q^2=q^2=0$), $E2$ is known to be at most a few percent of $M1$. Setting $E2=0$ we have

$$C_4(0)=C_3(0)/M_f. \quad \text{(A8)}$$

Hence

$$M1(q^2=0)=(2Q^*e/\sqrt{N})C_3(q^2=0). \quad \text{(A9)}$$

(4) The procedure of multipole decomposition described above can be applied to higher resonances. As long as the target particle has spin $\frac{1}{2}$, we have at most three multipoles no matter what the spin of the excited state may be. When the target particle has spin greater than $\frac{1}{2}$, $S_i>\frac{1}{2}$, we have more multipoles than three; but we will have more λ_i to choose from and hence will always have enough equations like (A2), (A3), and (A4) to determine all the multipoles.

The matrix element squared summed over λ_i and λ_f can then be written using Eq. (135.1) and Eq. (135.2) of DDM. In our example, we have

$$\sum_{\lambda_i\lambda_f}|\Gamma_{\lambda_f\lambda_i}{}^{(0)}|^2=\tfrac{1}{5}(Q2)^2, \quad \text{(A10)}$$

$$\sum_{\lambda_i\lambda_f}|\Gamma_{\lambda_f\lambda_i}{}^{(+)}|^2=\sum_{\lambda_f\lambda_i}|\Gamma_{\lambda_f\lambda_i}{}^{(-)}|^2=\sum_{\lambda_f\lambda_i}|\Gamma_{\lambda_f\lambda_i}{}^{(x)}|^2$$
$$=\sum_{\lambda_f\lambda_i}|\Gamma_{\lambda_f\lambda_i}{}^{(y)}|^2=\tfrac{1}{3}(M1)^2+\tfrac{1}{5}(E2)^2. \quad \text{(A11)}$$

These expressions can always be checked against the similar expressions obtained by using traces and projection operators. For example, in our case

$$\sum_{\lambda_f\lambda_i}|\Gamma_{\lambda_f\lambda_i}{}^{(x)}|^2$$
$$=-\mathrm{Tr}\frac{\boldsymbol{P}_i+M_p}{2M_p}\pi_\nu{}^{(x)}\gamma_5\frac{\boldsymbol{P}_f+M_f}{2M_f}\Big\{g_{\nu\mu}-\frac{2}{3}\frac{P_{f\mu}P_{f\nu}}{M_f{}^2}$$
$$+(1/3M_f)(P_{f\nu}\gamma_\mu-P_{f\mu}\gamma_\nu)-\tfrac{1}{3}\gamma_\nu\gamma_\mu\Big\}\gamma_5\pi_\mu{}^{(x)}, \quad \text{(A12)}$$

where

$$\pi_\nu{}^{(x)}=C_3(\boldsymbol{q}g_{\nu x}-q_\nu\gamma_x)+C_4(q\cdot P_f g_{\nu x}-q_\nu P_{fx})$$
$$+C_5(q\cdot P_i g_{\nu x}-q_\nu P_{ix}). \quad \text{(A13)}$$

It is probably worth mentioning that the method using Eqs. (A10) and (A11) takes much less effort than the one using Eq. (A12) unless the trace in the latter is taken by computer. We have used all methods checking both by hand calculations and by the computer program of Hearn.[24]

[24] A. C. Hearn, Commun. ACM 9, 573 (1966). See also "REDUCE User's Manual," Stanford Institute of Theoretical Physics Report No. ITP-247 (unpublished).

PHYSICAL REVIEW VOLUME 168, NUMBER 5 25 APRIL 1968

Free Massless Fields as Infinite-Dimensional Representations of the Lorentz Group*

CARL M. BENDER†
Harvard University, Cambridge, Massachusetts

(Received 1 September 1967; revised manuscript received 31 October 1967)

Free quantized massless field theories of arbitrary spin L are investigated. The transverse potential in the radiation gauge is shown to transform as a nonunitary infinite-dimensional representation of the Lorentz group: $(L,1)\oplus(L,-1)$ for integer spin and $(L+\frac{1}{2},\frac{1}{2})\oplus(L+\frac{1}{2},-\frac{1}{2})$ for integer $+\frac{1}{2}$ spin (Gel'fand and Shapiro's notation). Using Lorentz group theory, it is argued that free quantized massless field theories of spin >1 do not possess a stress-energy tensor $T^{\mu\nu}$.

I. INTRODUCTION

IN a recent paper,[1] Strocchi showed that the A potential in free-field quantum electrodynamics cannot transform as a vector, as it does in the classical theory. What, then, is its transformation law (if any), and is it unique?

It is the main purpose of this paper to elucidate this transformation law, not only for spin 1, but also for spin L. In Sec. II, the assumptions of this paper will be stated, and the radiation gauge will be precisely defined. In Sec. III, this definition will be used to prove the radiation gauge manifestly covariant; the transverse fields will be shown to belong to infinite-dimensional, nonunitary representations of the Lorentz group.

With this established, the simpler case of integer-spin massless-field theories will be developed. Section IV contains the derivation of the transformation law and the field equations of these theories and some remarks on the field strengths. Section V discusses some applications of the transformation law, such as the construction of scalar and tensor bilinear forms. In Sec. VI (Conclusions), the Lorentz invariance of the theory and the question of the Lagrangian in massless-field theories are discussed. It is concluded that canonically quantized Lagrangian massless-field theories of spin $L>1$ do not possess a covariant stress-energy tensor $T^{\mu\nu}$.

* Supported in part by Air Force Office of Scientific Research under Contract AF 49 (638)-1380.
† Supported by a National Science Foundation Predoctoral Fellowship.

[1] F. Strocchi, Phys. Rev. 162, 1429 (1967).

II. RADIATION GAUGE

Gauge invariance occurs in massless-field theories of spin $L>\frac{1}{2}$ because the field equations that are derived from a Lagrangian do not completely determine the fields. Gauge transformations leave invariant that part of the field which is determined.

The fields in the radiation gauge are called transverse. The radiation gauge is defined by stating the properties of these transverse fields [Eq. (1)].

For Bose-Einstein field theories of spin $L\geq 1$, $A(L)^L{}_{a_1\cdots a_L}$ is a Hermitian, totally symmetric, traceless tensor field, with a_i being 3-space indices,

$$\nabla_{a_i}A(L)^L{}_{a_1\cdots a_L}=0, \quad i=1,\cdots,L. \quad \text{(1a)}$$

The superscript L indicates that A has L indices. The L in parentheses indicates that A describes a spin-L theory.

For Fermi-Dirac field theories of spin $L+\frac{1}{2}\geq\frac{3}{2}$, $\psi(L+\frac{1}{2})^L{}_{a_1\cdots a_L}$ is a Hermitian, totally symmetric,